Non-Destructive Testing of Glass-Fibre Reinforced Polymers using Terahertz Spectroscopy

Frank RUTZ, Steffen WIETZKE, Martin KOCH, Institut für Hochfrequenztechnik, Braunschweig, Germany
Heike RICHTER, Stefan HICKMANN, Volker TRAPPE, Uwe EWERT, Federal Institute for Materials Research and Testing, Berlin, Germany

Abstract. We present THz time-domain spectroscopy measurements on glass-fibre reinforced polymers. The experimental set-up consists of a standard free-space THz spectrometer with photoconductive emitter and detector antennas driven by a femtosecond laser source. Single-point measurements to precisely obtain the THz properties of the sample are performed as well as two-dimensional images by scanning the samples perpendicular to the THz beam. We find that absorption coefficient and refractive index of the fibres significantly differ from that of the polymeric matrix material. Furthermore, the THz waves are strongly attenuated due to scattering off the fibres. The refractive index depends on the fibre concentration and orientation with respect to the linearly polarised THz radiation. With these results we can interpret THz images of a fibre reinforced polymer specimen. The THz images show the textures of the fibre network within the specimens and are compared with x-ray images.

Introduction

Fibre reinforced polymers and composites are increasingly used as constructional materials for their lightness and robustness. Yet, quality control of polymeric products are usually performed offline, i.e. with a certain distance and delay to the production process. Common offline methods are mechanical tests and light or scanning electron microscopy of sections. However, these methods merely cover random sampling which, therefore, are not perfectly reliable. Furthermore, the samples get destroyed. Possible non-destructive (and most of them also contactless) techniques include X-rays [1, 2], UV/VIS, NIR [3, 4], MIR, Raman spectroscopy [5], microwaves [6], NMR [7], thermography [8] and ultrasound [9]. An alternative to the already existing non-destructive testing (NDT) methods is the use of high-frequency electromagnetic radiation in the terahertz frequency range between 50 GHz and a few THz. Since THz waves can penetrate also stained polymers which are opaque in the visible, THz spectroscopy promises to be a powerful tool in process and quality control.

Meanwhile, there are several ways to generate THz radiation, e.g. gas lasers, backward-wave oscillators [10] and quantum cascade lasers [11, 12] to name just a few. Here, we utilise photoconductive switching with optical femtosecond laser pulses. The advantage of this time-domain spectroscopy (TDS) technique lies in the availableness of a wide bandwidth and the temporal (or phase) information. We present first THz TDS measurements on glass-fibre (GF) reinforced polymers.

1. THz Time-domain Spectroscopy

1.1 Experimental Set-up

Time-resolved terahertz spectroscopy is a rather novel technique [13]. This technique relies on ultra-short current pulses which are generated by femtosecond laser pulses in photoconductive dipole antennas. These current pulses act as a source for broadband THz pulses which are received by a second antenna of similar design [14-16]. The sample under investigation is placed in an intermediate focus between emitter and receiver antenna (see Figure 1). The THz waveform is scanned by delaying the two laser pulses in the emitter and detector arm with respect to each other. Thus, the laser pulse gating the detector antenna samples the incident THz waveform for a series of time delays. In order to obtain the absorption spectrum of the sample the frequency content of the transmitted THz pulse is compared to a reference spectrum.

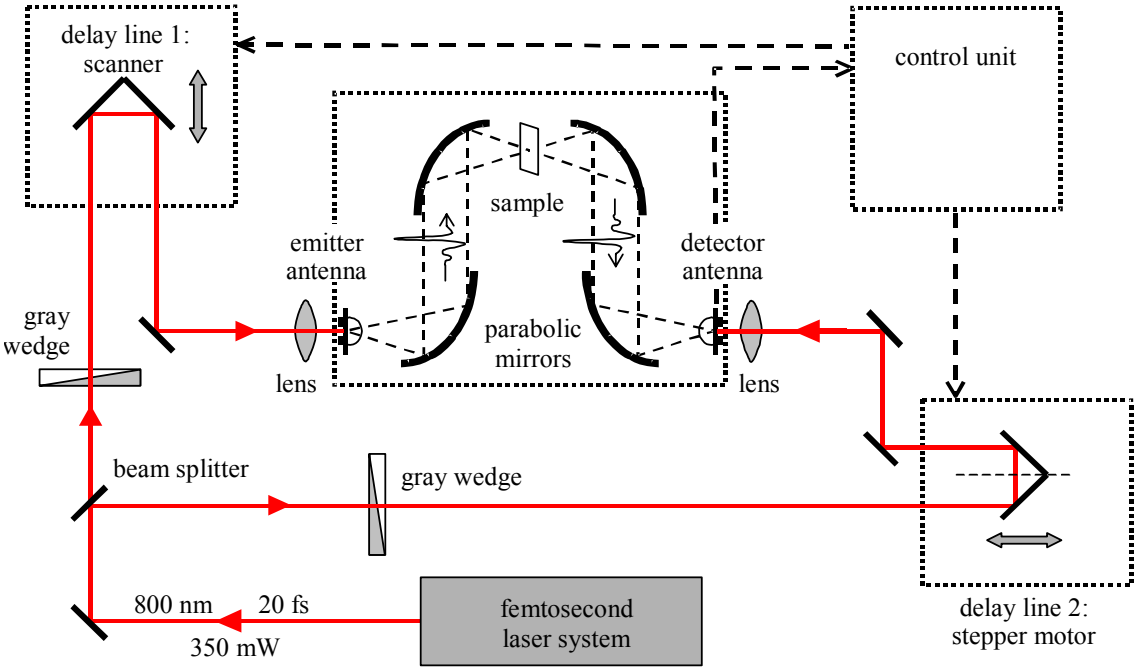

Figure 1. Schematic of the applied THz time-domain spectrometer

1.2 Measurement Technique

THz TDS is named after the fact that the experimentally obtained data are temporal data curves, i.e. time-domain data $E(t)$. The frequency-domain data $F(\omega)$ are obtained from the time-domain data by a numerical Fourier transform algorithm (FFT). Since the THz pulse basically resembles a single "optical" cycle, the spectral power distribution covers a broad frequency range due to the Fourier principle (see Figure 2). By comparing the complex Fourier spectra of two consecutive measurements with and without a sample inserted in the spectrometer, denoted with "sample" and "reference", the material parameters absorption coefficient α and refractive index n of the sample are determined.

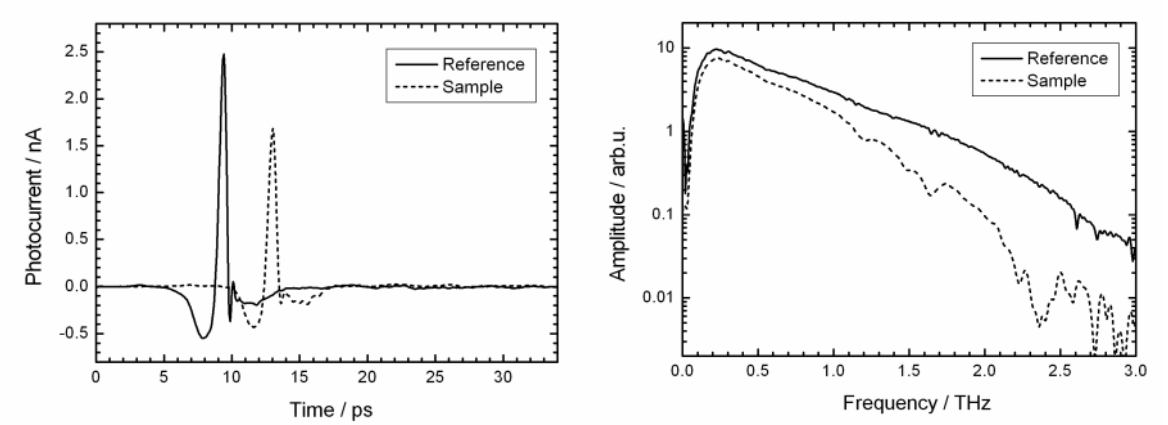

Figure 2. THz waveforms (a) measured with a sample (dashed) and without any sample (solid line) placed in the spectrometer. The corresponding frequency amplitude spectra (b) obtained by Fourier transform algorithm (FFT) yield information about the transmission characteristics of the sample.

With $F_{sample}(\omega) / F_{reference}(\omega) = T(\omega) \exp(i\Delta\varphi(\omega))$, T is the relative amplitude transmission and $\Delta\varphi$ the absolute phase shift of the sample. The refractive index and absorption coefficient of the sample with the thickness d are calculated via $n(\omega) = 1 + c_0 \Delta\varphi(\omega) / (\omega d)$ and $\alpha(\omega) = -2/d \ln\{T(\omega) [n(\omega) + 1]^2 / [4 n(\omega)]\}$. c_0 denotes the speed of light in vacuum.

Most polymers are widely transparent in the THz region and can easily be "t-rayed". This applies also for coloured plastic products that are opaque in the visible or infrared range, whereas several additives like glass-fibres, carbon black or magnesium hydroxide show significantly increased absorption. Eventually, due to the large wavelength of some hundred micrometres, which often lies in the range of the fibre dimensions, the THz frequency range provides different contrast mechanisms as compared to near-infrared, visible or X-ray radiation. These contrast mechanisms are unique, and hence, open up tremendous technological opportunities [17]. Moreover, in contrast to X-rays, THz radiation is not ionising due to its low photon energy and is therefore completely harmless [18].

Since THz TDS employs electromagnetic pulses, analogies to ultrasound can be drawn. Differences in the temporal delay of the propagated pulses or the temporal positions of their echoes deliver information on the thickness and on the inner structure of the polymer objects. Hence, internal interfaces, material inhomogeneities, and trapped air cavities can be detected [14, 17]. For example, two different polymers which both have low absorption coefficients usually differ in their refractive indices. If there is not an ideal mixture of single components within a compound the temporal position of the transmitted THz pulse should vary over the sample as well.

By scanning the sample in two dimensions (x,y) perpendicular to the beam through the intermediate THz focus a THz image can be obtained [14, 15, 19, 20]. Each pixel represents one certain value resulting from the analysis of the transmitted THz waveform at the corresponding sample position. This can be the transmitted power in the full frequency range or a certain interval or just the temporal position of the pulse maximum [20]. Since all these values can be computed automatically a single imaging measurement yields many THz images.

2. Samples

2.1 Fibre Concentration Series

In order to determine the influence of fibre reinforcement on the THz material parameters of polymers we first investigated a series of 2 mm thick planar samples with various GF concentrations. The matrix polymer consists of polyamide (PA66) "Ultramid A3" (BASF) coloured black by the addition of some carbon black which is quite common in the plastics industry. The test series comprised composites containing 0 (pure polymer), 15, 30, 45 and 60 wt% glass-fibres "Cratec$^{\underline{\text{Plus}}}$ 173X" (Owens Corning). With the conversion from weight fraction w to volume fraction v via $v_{GF} = w_{GF} / (w_{GF} + w_{PA}\ \rho_{GF}/\rho_{PA})$, with the specific densities ρ_{GF} and ρ_{PA} of the GFs and the matrix polymer, respectively, this corresponds to 0, 7.3, 16.1, 26.8 and 40.2 vol%. Every specimen was measured at three different positions to ensure reproducibility.

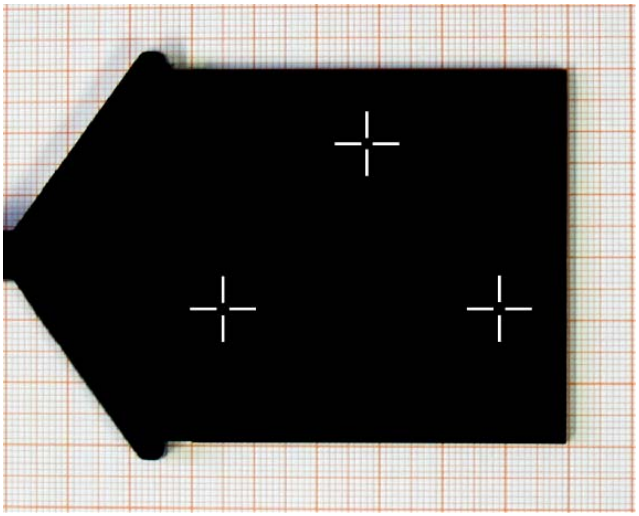

Figure 3. Photograph of a injection moulded GF/PA66 composite specimen. Three marks indicate the measurement spots.

2.2 Fibre Network Composite

A second kind of sample consists of a GF reinforced tensile specimen made from an epoxy matrix with included eight 250 µm thick layers of woven GF fabrics of linen-style as a +/–45°-laminate. This specimen is fractured since it has already been tested in tensile loading. The matrix material epoxy is a resin, which in the cured state is a duroplastic polymer. The fibre reinforcement is stabilised in position by the matrix which yields a composite of a low weight as well as a high mechanical and chemical stability. With unidirectional reinforcement GF composites can reach up a tensile strength of about 700 to 1000 MPa. The direction of the fibre reinforcement depends on the purpose of use for the decisive component. A +/–45°-laminate is utilized for parts which exhibit shearing strains.

3. Results and Discussion

3.1 THz TDS of Fibre Concentration Series

With the first set of samples, we investigated how the GF content influences the THz properties of polymeric composites. Figure 4 (a) shows the results for the frequency dependent refractive index *n* for the GF mass fractions 0, 15, 30, 45 and 60 wt%. Each curve is obtained by averaging over three independent measurements at different spots of the sample. No spectral features occur but a clear increase of the overall refractive index can be observed for rising GF contents. Plotting *n* averaged over frequency against the volume fraction *v* yields the graph in Figure 4 (b). There is a excellent linear dependency between *n* and *v*, with $n(v) = 1.75$ (pure PA66) + 0.83 *v*/vol%. Extrapolating this to 100 vol% results in a theoretical value for the refractive index for GFs of $n(\mathrm{GF}) = 2.58$. There is also an increase of the absorption coefficient α integrated over frequency (0.17 – 0.75 THz) for rising *v*. However, the dependency is not as pronounced as for the refractive index.

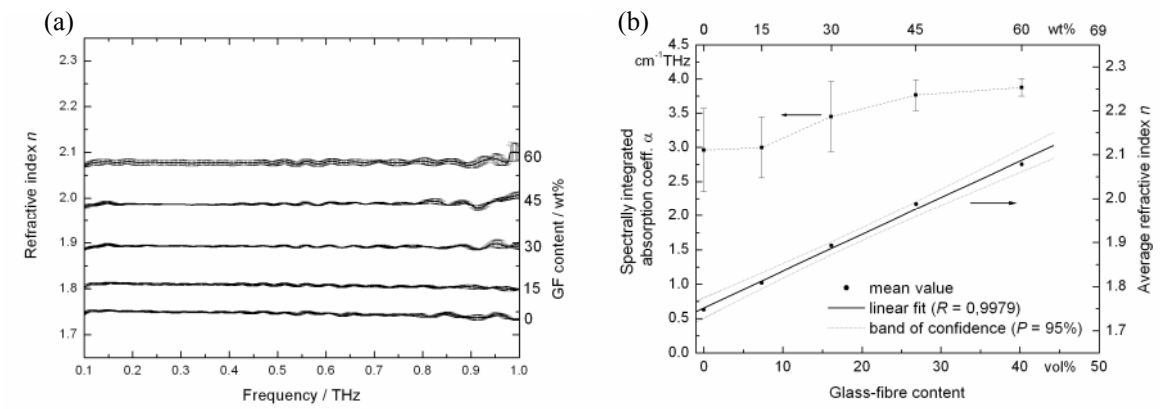

Figure 4. Measurement results of several GF/PA66 composite samples with different GF contents. (a) Frequency dependent refractive index, (b) spectrally integrated absorption coefficient and average refraction index against fibre concentration.

All the abovementioned measurements were performed with the same orientation of the samples. Since the samples were ejection moulded and fibres with a high aspect ratio (length over diameter) tend to align along the flow direction, the orientation of the sample with respect to the THz polarisation might influence the experimental results. Thus, one sample (30 wt% GF) was measured in a different orientation, i.e. 90° rotated. The results are shown in Figure 5. The refractive index (a) reveals a slight birefringence of the composite with an index change of 0.02 between parallel and perpendicular polarisation. Regarding the absorption coefficient (b) no significant polarisation effects can be observed. Since pure PA66 does not provide any orientation dependency the birefringence definitely arises from the GFs.

As a summary of these findings, with THz TDS one can determine the local GF concentration within a composite without destroying or even contacting the sample. Furthermore, for known concentrations even the fibre orientation can be determined by measuring the refractive index.

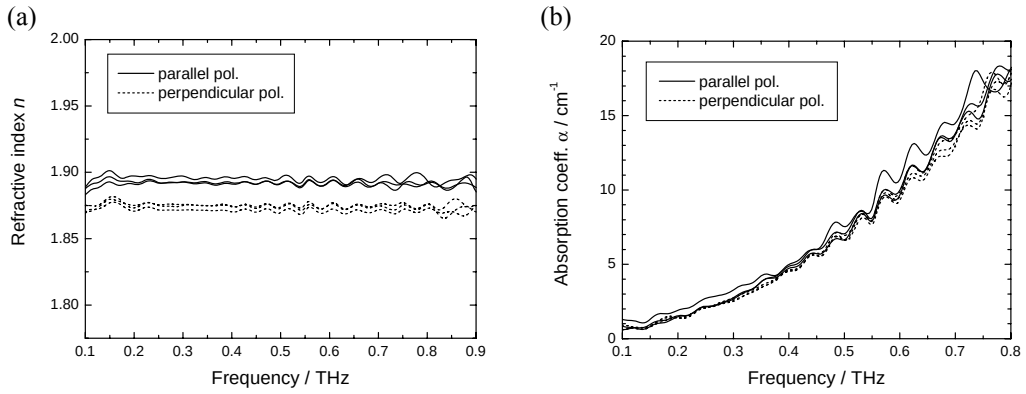

Figure 5. Frequency dependent refractive index (a) and absorption coefficient (b) of 30 wt% GF/PA66 composite. A slightly higher refractive index occurs if the THz radiation is polarised parallel with the overall fibre orientation compared to the perpendicular polarisation. No such distinction can be found in the absorption coefficient.

3.2 THz Imaging of Fibre Network Composite

With THz imaging heterogeneities within planar samples can be investigated. The fractured tensile specimen is an ideal test sample for imaging measurements as the photograph of the sample in Figure 6 (a) and 7 (a) already shows various features and patterns. The THz imaging data are illustrated in Figure 6 (b) and (c).

In Figure 6 (b) which shows the transmitted intensity of the frequency interval 0.3 – 0.4 THz cloudy features are observed which are not one-to-one found in the photograph. However, in the frequency interval 0.5 – 0.75 THz the linen-style pattern of the GF fabric emerges (Figure 6 (c)). This can be explained since the wavelength of higher THz frequencies is smaller and, therefore, the texture can be resolved. The reason for the cloudy features, which remain visible in this image, is not fully understood. We attribute them to damages that have arisen from the tensile loading that led to the break of the specimen. The light-coloured regions in the photograph indicate where the first GF layer has delaminated. Such delaminations have very likely occurred between the underlying layers, too. The resulting cavities can lead to interference which strongly effect the apparent THz transmission.

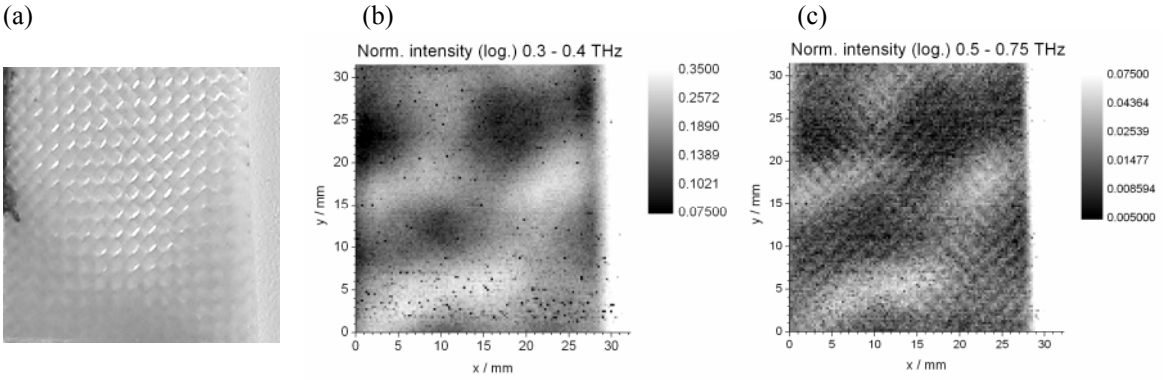

Figure 6. Photograph (a) of the tensile specimen with corresponding THz transmission images for the integrated intensity in the interval 0.3 – 0.4 THz (b) and 0.5 – 0.75 THz (c).

3.3 Comparison with X-ray Images

To compare THz imaging with already established X-ray techniques, small angle X-ray scattering (SAXS) images have been measured [21, 22]. Figure 7 (b) represent the C_m/μ image derived from the absorption and the refraction channel. The image reproduces the GF fabric very slightly. In the upper part of the SAXS image (b), which coincides with the light-coloured regions in the photograph (a), much more radiation is scattered off the primary beam into the detector. As the refracted intensity is a measure for the specific inner surface of the sample, enhanced microcracking and delamination probably causes the formation of tiny cavities the interfaces of which sum up to increased inner surface values [21, 22]. This is consistent with the interpretation of the THz images above.

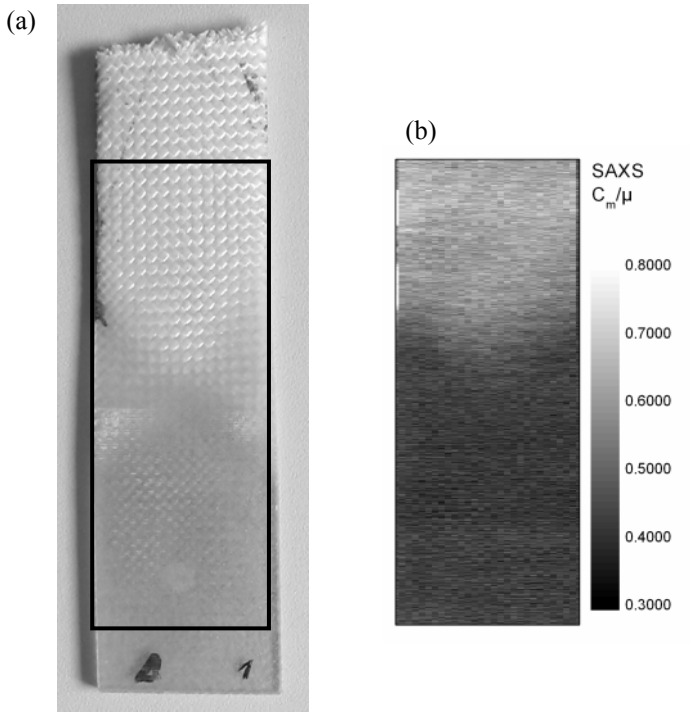

Figure 7. Photograph (a) of the tensile specimen. The frame indicates the area of the SAXS image (b).

4. Conclusions

We have presented THz TDS measurements of two kinds of GF reinforced polymers. For a series of GF/PA66 composites with various GF contents the influence of GF on the THz properties of the composite was investigated. We found a linear dependency of the refractive index on the GF volume fraction. Furthermore, the refractive index changed for different THz polarisations with respect to the overall fibre orientation.

We have also performed THz imaging of a fractured GF/epoxy tensile specimen. Beside the texture of linen-style GF fabric we detected heterogeneities which are attributed to microcracking and delamination defects that arose from the tensile loading. A comparison with a SAXS image supported the interpretation of the THz images.

In summary, the power of THz TDS as a non-destructive and contactless testing technique for GF reinforced polymers was demonstrated.

Acknowledgment

This work was supported by the Federal Ministry for Economics and Technology (BMWA) through the Arbeitsgemeinschaft industrieller Forschungsvereinigungen "Otto von Guericke" e.V. (AiF) project 182 ZN. We highly appreciate the financial support. We would also like to thank the Süddeutsches Kunststoffzentrum (SKZ) in Würzburg, Germany, and the Federal Institute for Materials Research and Testing (BAM) in Berlin, Germany, for providing the samples.

References

[1] L.E. Alexander, *X-ray diffraction methods in polymer science,* Wiley-Interscience, New York, London, Sydney, Toronto (1969).
[2] R.-J. Roe (ed.), *Methods of X-Ray and Neutron Scattering in Polymer Science,* Oxford Univ. Press, New York (2000).
[3] T. Rohe, W. Becker, A. Krey, H. Nägele, S. Kölle, N. Eisenreich, *In-line monitoring of polymer extrusion processes by NIR spectroscopy*, J. Near Infrared Spectr. **6**, 325-332 (1998).
[4] A.F. Santos, E.L. Lima, J.C. Pinto, *In-Line Evaluation of Average Particle Size in Styrene Suspension Polymerization Using Near Infrared Spectroscopy*, J. Appl. Polym. Sci. **70**, 1737-1745 (1998).
[5] K. Ito, T. Kato, T. Ona, *Non-destructive method for the quantification of the average particle diameter of latex as water-based emulsions by near-infrared Fourier transform Raman spectroscopy*, J. Raman Spectroscopy **33**, 466-470 (2002).
[6] D. Hughes, M. Kazemi, K. Marler, R. Zoughi, J. Myers, A. Nanni, *Microwave detection of delaminations between fiber reinforced polymer (FRP) composite and hardened cement paste,* AIP Conf. Proc. **615** (1), 512-519 (2002).
[7] J.C. Randall, *Polymer sequence determination: carbon-13 NMR method,* Academic Press, New York, London (1977).
[8] J.M. Levar, H.R. Hamilton, Nondestructive Evaluation of Carbon Fiber-Reinforced Polymer-Concrete Bond Using Infrared Thermography, ACI Mat. J. 100-M8, 63-72 (2003).
[9] R. Gendron, J. Tatibouët, J. Guèvremont, M. M. Dumoulin, L. Piché, *Ultrasonic behavior of polymer blends,* Polym. Eng. Sci. **35** (1), 79-91 (1995).
[10] G.A. Blake, K.B. Laughlin, R.C. Cohen, K.L. Busarow, D-H. Gwo, C.A. Schmuttenmaer, D.W. Steyert, R.J. Saykally, *Tunable far infrared laser spectrometers,* Rev. Sci. Instrum. **62** (7), 1693-1700 (1991).
[11] G. Gagliardi, S. Viciani, M. Inguscio, P. De Natale, C. Gmachl, F. Capasso, D.L. Sivco, J.N. Baillargeon, A.L. Hutchinson, A.Y. Cho, *Generation of tunable far-infrared radiation with a quantum cascade laser,* Opt. Lett. **27** (7), 521-523 (2002).
[12] H.-W. Hübers, S.G. Pavlov, A.D. Semenov, R. Köhler, L. Mahler, A. Tredicucci, H.E. Beere, D.A. Ritchie, E.H. Linfield, *Terahertz quantum cascade laser as local oscillator in a heterodyne receiver,* Opt. Express **13** (15), 5890-5896 (2005).
[13] D.M. Mittleman (ed.), *Sensing with Terahertz Radiation*, Springer, Heidelberg (2003).
[14] S. Hunsche, D.M. Mittleman, M. Koch, M.C. Nuss, *New Dimensions in T-Ray Imaging*, IEICE Trans. Electron., E81-C, 269-276 (1998).
[15] D.M. Mittleman, M. Gupta, R. Neelamani, R.G. Baraniuk, R.G. Rudd, M. Koch, *Recent Advances in Terahertz Imaging*, Appl. Phys. B **68**, 1085-1094 (1999).
[16] M. Koch, L. Beckmann, F. Rutz, P. Knobloch, T. Kleine-Ostmann, K. Pierz, G. Hein, H. Niemann, B. Güttler, *Sensing with THz imaging*, VDI-Berichte **1844**, 11-22 (2004).
[17] C. Zandonella, *T-ray specs*, Nature **424**, 721-722 (2003).
[18] G.P.Gallerano, *Tera-Hertz radiation in Biological Research, Investigations on Diagnostics and study on potential Genotoxic Effects*, EU-Study "THz-Bridge", final report (2004).
[19] B.B. Hu, M.C. Nuss, *Imaging with terahertz waves*, Opt. Lett. **20**, 1716-1718 (1995).
[20] M. Herrmann, M. Tani, K. Sakai, *Display Modes in Time-Resolved Terahertz Imaging*, Jpn. J. Appl. Phys. **39**, 6254-6258 (2002).
[21] V. Trappe, M. Hentschel, H. Ivers, *Micro-mechanical properties of fiber composites characterized by X-ray refraction,* Proc. SPIE Int. Soc. Opt. Eng. **5766**, 15-24 (2005).
[22] V. Trappe, K.-W. Harbich, *Intralaminar fatigue behaviour of carbon fibre reinforced plastics,* Int. J. Fatigue, in press (2006).